Cancer Research

Calreticulin Expression in Human Non–Small Cell Lung Cancers Correlates with Increased Accumulation of Antitumor Immune Cells and Favorable Prognosis

Jitka Fucikova[1,2], Etienne Becht[3,4,5], Kristina Iribarren[3,4,5], Jeremy Goc[3,4,5], Romain Remark[3,4,5], Diane Damotte[3,4,5,6], Marco Alifano[7], Priyanka Devi[3,4,5], Jerome Biton[3,4,5], Claire Germain[3,4,5], Audrey Lupo[3,4,5,6], Wolf Herve Fridman[3,4,5], Marie-Caroline Dieu-Nosjean[3,4,5], Guido Kroemer[3,4,5,8,9,10,11], Catherine Sautès-Fridman[3,4,5], and Isabelle Cremer[3,4,5]

Abstract

A high density of tumor-infiltrating mature dendritic cells (DC) and $CD8^+$ T cells correlates with a positive prognosis in a majority of human cancers. The recruitment of activated lymphocytes to the tumor microenvironment, primed to recognize tumor-associated antigens, can occur in response to immunogenic cell death (ICD) of tumor cells. ICD is characterized by the preapoptotic translocation of calreticulin (CRT) from the endoplasmic reticulum (ER) to the cell surface as a result of an ER stress response accompanied by the phosphorylation of eukaryotic initiation factor 2α (eIF2α). We conducted a retrospective study on two independent cohorts of patients with non–small cell lung cancer (NSCLC) to investigate the prognostic potential of CRT. We report that the level of CRT expression on tumor cells, which correlated with eIF2α phosphorylation, positively influenced the clinical outcome of NSCLC. High CRT expression on tumor cells was associated with a higher density of infiltrating mature DC and effector memory T-cell subsets, suggesting that CRT triggers the activation of adaptive immune responses in the tumor microenvironment. Accordingly, patients with elevated CRT expression and dense intratumoral infiltration by DC or $CD8^+$ T lymphocytes had the best prognosis. We conclude that CRT expression constitutes a new powerful prognostic biomarker that reflects enhanced local antitumor immune responses in the lung. *Cancer Res; 76(7); 1746–56. ©2016 AACR.*

[1]Department of Immunology, Charles University, 2nd Faculty of Medicine and University Hospital Motol, Prague, Czech Republic. [2]Sotio, Prague, Czech Republic. [3]Institut National de la Santé et de la Recherche Médicale (INSERM), UMRS1138, Centre de Recherche des Cordeliers, Paris, France. [4]Université Pierre et Marie Curie-Paris 6, UMRS1138, Paris, France. [5]Université Paris Descartes-Paris 5, UMRS1138, Paris, France. [6]Service d'Anatomie-Pathologique, Hôpital Hotel Dieu, AP-HP, Paris, France. [7]Service de Chirurgie Thoracique, Hôpital Cochin, AP-HP, Paris, France. [8]Metabolomics and Cell Biology Platforms, Gustave Roussy, Villejuif, France. [9]Equipe 11 labellisée Ligue contre le Cancer, Centre de Recherche des Cordeliers, INSERM UMRS 1138, Paris, France. [10]Pôle de Biologie, Hôpital Européen Georges Pompidou, AP-HP, Paris, France. [11]Karolinska Institute, Department of Women's and Children's Health, Karolinska University Hospital, Stockholm, Sweden.

Note: Supplementary data for this article are available at Cancer Research Online (http://cancerres.aacrjournals.org/).

Current address for J. Goc: Joan and Sanford I. Weill Department of Medicine, Division of Gastroenterology and Hepatology, Department of Microbiology and Immunology and The Jill Robert's Institute for Research in Inflammatory Bowel Disease, Weill Cornell Medicine, Cornell University, 413 East 69th Street, Belfer Research Building 712, Box 210, New York, NY 10021; and current address for R. Remark, Division of Hematology and Oncology, The Tisch Cancer Institute, Icahn School of Medicine at Mount Sinai, New York, NY.

Corresponding Author: Isabelle Cremer, Institut National de la Santé et de la Recherche Médicale (INSERM), UMRS 1138, Centre de Recherche des Cordeliers, 15 rue de l'Ecole de Médecine, Paris 75006, France. Phone: 331-4427-9083; Fax: 331-4051-0420; E-mail: isabelle.cremer@crc.jussieu.fr

doi: 10.1158/0008-5472.CAN-15-1142

Introduction

Recent advances in tumor biology have highlighted the complex interplay between the immune system and tumor and have revealed the major role of the adaptive immune system in the control of tumor growth (1, 2). The tumor microenvironment consists in a complex network of malignant, stromal, and immune cells. Tumor-infiltrating immune cells have been described in most solid tumors (3, 4). The type, the density, and the location of immune cells in the tumor microenvironment, defined as immune contexture strongly affect the prognosis of cancer patients (4–7). In non–small cell lung cancer (NSCLC), a high density of mature dendritic cells (DC) correlates with long-term survival of the patients (8) and with a strong infiltration by $CD8^+$ T cells that are predominantly of the effector-memory phenotype (9). Within the group of patients with high densities of $CD8^+$ T cells, those with few mature DCs exhibit lower overall survival (OS) than those with high densities of mature DCs, suggesting that tumor-infiltrating $CD8^+$ T cells may be functionally heterogenous (9, 10).

The immunogenicity of cancer cells results from their antigenicity, (i.e., the expression of specific tumor antigens) and their adjuvanticity, (i.e., the expression or release of danger-associated molecular patterns or DAMP). One particular way to deliver DAMPs into the tumor microenvironment is immunogenic cell death (ICD), a functionally peculiar type of apoptosis

AACR

that stimulates tumor-specific immune responses (11–14). The immunogenicity of cell death relies on at least three independent events, namely (i) the preapoptotic exposure of the endoplasmic reticulum (ER) chaperone protein calreticulin (CRT; refs. 15, 16) and perhaps other chaperones such as HSP70 and HSP90 (17), at the cell surface, (ii) the subsequent autophagy-dependent active secretion of adenosine triphosphate (ATP; refs. 3, 18, 19) and (iii) the postapoptotic release of the nuclear nonhistone chromatin-binding protein high mobility group box 1 (HMGB1; refs. 20, 21). By binding to CD91 on the surface of DCs, CRT functions as an "eat-me" signal, thus promoting the engulfment of apoptotic bodies by DCs (22). Knockdown of CRT, blockade of ecto-CRT, or inhibition of the pathway leading to CRT exposure abolishes the immunogenicity of cell death (19, 23). These findings suggest that DAMPs can stimulate antigen presenting cells, particularly DCs, to efficiently engulf dying cells, process antigens, mature, and induce an efficient immune response.

Most studies on ICD have focused on experimental mouse models (19, 20, 23–28) and *in vitro* human studies (15, 17, 19, 20, 23–33), but large-scale studies are necessary to determine the prognostic value of ICD-associated DAMPs expression, as well as their role in cancer immunosurveillance in patients. Here, we investigated the clinical impact of CRT expression on two independent cohorts of operable NSCLC patients having received neoadjuvant chemotherapy or not. Using IHC on operative specimen, we demonstrate that CRT is a powerful prognostic factor for OS of NSCLC patients, which were either treated by neoadjuvant chemotherapy or left without treatment, even after correcting for pathologic stage. Furthermore, we evaluated whether expression of CRT is associated with an enhanced cellular immune response. We identified a statistically significant correlation between expression of CRT and density of mature DCs, but not with $CD8^+$ T cells, B cells, and macrophages. We showed on fresh resected tumors that exposure of CRT occurs specifically at the cell surface of tumor cells and is strongly associated with the presence of effector memory T cells in the tumor microenvironment.

Patients and Methods

Patients

Study group 1. A retrospective series of 270 stage I to III–IV NSCLC patients who underwent primary surgery (without neoadjuvant chemotherapy) and who were operated between 2001 and 2005 was obtained from Hotel-Dieu Hospital (Paris, France). Baseline characteristics of these patients are summarized in Table 1.

Study group 2. A retrospective cohort of 125 stage III-N2 NSCLC patients who received neoadjuvant chemotherapy followed by curative resection between 2000 and 2007 was obtained from Hotel-Dieu Hospital. Baseline characteristics of these patients are summarized in Supplementary Table S2.

Pathologic staging of lung cancer was reviewed and classified according to the new TNM classification 2009 (34), and histologic types were determined according to the WHO classification (35).

Study group 3. A prospective series of 50 NSCLC patients was obtained from Cochin-Hotel-Dieu Hospital and Institute Mutualiste Montsouris (Paris, France). These patients underwent primary surgery in 2013.

Informed consent was obtained for each patient after the nature and possible consequences of the studies were explained and lung tumor samples were analyzed with the agreement of the French ethical committee (agreement 2008-13 and 2012 06-12) in accordance with the article L.1121-1 of French law.

Table 1. Clinical characteristics of NSCLC patients not treated with neoadjuvant chemotherapy, with CRT^{Hi} versus CRT^{Lo} tumors

	Overall cohort ($n = 270$)	**CRT^{Hi} ($n = 239$)**	**CRT^{Lo} ($n = 31$)**	***P***
Gender				
Male	227 (84%)	200 (84%)	27 (87%)	0.8
Female	43 (16%)	39 (16%)	4 (13%)	
Age				
Mean (years) ± SEM	64 ± 0.04	64 ± 0.04	64 ± 0.4	0.9
Smoking history				
Smoker	232 (86%)	205 (86%)	27 (87%)	
Never smoker	33 (12%)	31 (13%)	2 (6.5%)	0.55
NA	5 (2%)	3 (1%)	2 (6.5%)	
Histologic type				
ADC	143 (53%)	126 (53%)	17 (55%)	
SCC	101 (37.5%)	92 (39%)	9 (29%)	0.36
Others	15 (5.5%)	12 (5%)	3 (9.5%)	
NA	11 (4%)	9 (3%)	2 (6.5%)	
Stage of disease				
Stage I	112 (41%)	103 (43%)	9 (29%)	
Stage II	75 (28%)	64 (27%)	11 (35.5%)	0.28
Stage III–IV	83 (31%)	72 (30%)	11 (35.5%)	
P.eiF2α score	4 ± 0.0058	4 ± 0.0058	2.6 ± 0.092	**0.0067**
Immune infiltrate				
DC-LAMP density	1 ± 0.013	1.1 ± 0.016	0.62 ± 0.048	**0.042**
CD8 density	360 ± 1.8	370 ± 2	320 ± 12	0.15

NOTE: All clinical parameters were evaluated among the 270 NSCLC patients. Age at the date of the surgery is reported. DC-LAMP and CD8 T-cell densities (counted on the whole slide) were evaluated among 241 and 235 patients, respectively. P-eiF2α score was evaluated among 164 patients. Significant association to CRT stratification (based on the optimal *P* value approach to determine CRT^{Hi} and CRT^{Lo} groups) was assessed using Mann–Whitney or Fisher exact tests. Bold, $P < 0.05$. Abbreviations: ADC, adenocarcinoma; SCC, squamous cell carcinoma; NA, not available.

IHC

In the study groups 1 and 2, tumor samples were fixed in neutral buffered 10% formalin solution and paraffin-embedded. For each paraffin-embedded lung tumor, two observers (M.-C. Dieu-Nosjean and D. Damotte) selected the tumor section containing a representative area of tumor with adjacent lung parenchyma, and the highest density of immune cells on the hematoxylin and eosin-safran–stained tissue section. CRT, P-eIF2α, CD8, Ki67, DC-LAMP, CD20, CD68, and MHC-I immunostaining were conducted as follows, using the avidin–biotin–peroxidase complex method. Paraffin section was dewaxed, followed by antigen retrieval with Target Retrieval Solution (Dako), 10 μmol citrate buffer at pH 6.0 (for CRT, MHC-I, and CD68), in TRIS EDTA pH 9 (for P-eIF2α) or pH 8 (for CD8/Ki-67 double labeling) in a preheated water bath (98°C, 30 minutes). Sections were cooled at room temperature for 30 minutes and endogenous peroxidase was blocked with 3% hydrogen peroxide. Thereafter, sections were incubated with diluted 5% human serum for 30 minutes and incubated with mouse anti-human CRT mAb (clone FMC75, Abcam, 5 μg/mL), rabbit anti-human P-eIF2α mAb (clone E90, Abcam, 5 μg/mL), mouse anti-human MHC-I (clone ab70328, Abcam, 1/7,000), mouse anti-human CD68 (clone PGM1, Dako, 0.6 μg/mL) for 2 hours at room temperature. Peroxidase-linked secondary antibodies (Dako) and AEC (3-amino-9-ethylcarbazole) or DAB (3,3′-diaminobenzidine, Dako) were used to detect specific binding.

For CD8/Ki67 double labeling, slides were incubated rabbit anti-human CD8 (clone SP16, Spring Bioscience, 1/100) and mouse anti-human Ki67 (clone MIB-1, Dako, 0.35 μg/mL) for 2 hours at room temperature, followed by incubation with biotinylated donkey anti-rabbit and uncoupled goat anti-mouse (Jackson Immunoresearch), then by incubation with HRP–streptavidin (Dako, 2.6 μg/mL) and APAAP (phosphatase-anti-alkaline phosphatase, Dako, 3.48 μg/mL). AEC and alkaline phosphatase substrate (Vector laboratories) were used to detect specific staining.

CD8, DC-LAMP, and CD20 staining was performed as described previously (9, 36). For CD8, double labeling with AE1/AE3 was performed.

Methods for cell quantification

The expression level of CRT and P-eIF2α for each patient was determined as the score of positive tumor cells. The score index was calculated for 10 different fields at 20× magnification under a light microscope (Nikon eclipse, 80i) and classified into 5 scores (score 1: 10%–20% positive cells evaluated, score 2: 21%–40% positive cells, score 3: 41%–60% positive cells, score 4: 61%–80% positive cells, and score 5: 80%–100% positive cells). The quantification was done by two independent observers (J. Fucikova and I. Cremer), and reviewed by an expert pathologist (D. Damotte). The expression level of MHC-I was determined as the average percentage of MHC-I expression by tumor cells for 10 fields at 20× magnification under a light microscope (Nikon eclipse, 80i), by two independent readers (K. Iribarren and I. Cremer).

The quantification of DC-LAMP, CD8, CD20, and CD68 was performed as described previously (9, 36). Images were acquired using Nanozoomer (Hamamatsu) operated with NDPview software; $CD8^+$ and DC-$LAMP^+$, $CD20^+$, and $CD68^+$ cells were quantified in the stroma and the tumor nests of the whole tumor section with Calopix software (Tribvn), and expressed as an absolute number of positive cells/mm^2 of tumor for DC-LAMP, CD8, and CD68. Both immunostaining and quantification were reviewed by at least three independent observers (J. Goc, P. Devi, C. Germain, M.-C. Dieu-Nosjean). The number of $CD8^+Ki67^+$ cells was determined by counting double positive cells on the whole slide under a light microscope.

Immunofluorescence

For the detection of CRT, the cells were placed on ice, washed twice with PBS, and fixed in 0.25% paraformaldehyde in PBS for 5 minutes. The cells were then washed twice in PBS, and a primary anti-CRT antibody (clone FMC75, Enzo) or isotype control and anti-Na^+-K^+ATPase α1 antibody (Santa Cruz Biotechnology) diluted in cold blocking buffer was added for 30 minutes. After two washes in cold PBS, the cells were incubated for 30 minutes with the appropriate secondary antibody Alexa Fluor 488 IgG1 (Life Technologies) and Alexa Fluor 594 donkey anti-mouse IgG (H+L), respectively. The cells were fixed with 4% paraformaldehyde for 20 minutes, washed in PBS for 20 minutes, and mounted on slides.

Flow cytometry

Fresh lung tumor specimens and distant nontumoral tissues (taken at more than 10 cm of the tumor) were mechanically (manual) dissociated and digested in the presence of Cell Recovery Solution (BD Biosciences). Total live mononuclear cells were isolated from the tumors, as described previously (9), using Ficoll density-gradient separation. Briefly, cells from pellet remaining after Ficoll separation were incubated with primary antibodies against CD45, cytokeratin, human epithelial antigen, CD227 to distinguish the population of leukocytes, stromal, and epithelial cells, and antibodies against CRT (clone FMC75, Enzo) or isotype control, for 30 minutes at 4°C. Cells were washed and stained with Alexa 648–conjugated monoclonal secondary antibody for 30 minutes at 4°C. After washing, cell viability was assessed by AnnexinV PE (BD Pharmigen) or Live/Death Yellow staining (Life Technologies) and DAPI. For the characterization of immune cell population, mononuclear cells were stained with multiple panels of antibodies conjugated to fluorescent dyes and isotype controls (see Supplementary Table S1). Briefly, mononuclear cells were incubated with the primary antibodies for 30 minutes at 4°C in the dark. Cells were washed and analyzed on a LSRII cytometer (BD Biosciences) and FlowJo (TreeStar, Inc.) software.

Statistical analyses

Survival analysis was performed using the "survival" R package, using both log-rank tests and Cox proportional hazards regressions. When using a log-rank test, prognostic value of continuous variables was assessed using a median-based cutoff, or the optimal *P* value approach (Supplementary Fig. S1). In the latter case, *P* values were corrected using the technique proposed by Altman and colleagues (37). For Cox proportional hazards regressions, immune densities were log-transformed. In multivariate Cox regressions, variables that were not significantly associated with prognosis in univariate analysis (Wald test $P > 0.05$) were not included, as well as variables intrinsically correlated (for instance, continuous CRT variable was prioritized over dichotomized CRT). For linear correlation, orthogonal regression was used to plot the regression line, as noise is assumed to equally affect both CRT and P-eIF2α. Fisher exact test, Student *t* test, Wilcoxon, and Mann–Whitney tests were used to test for association between variables.

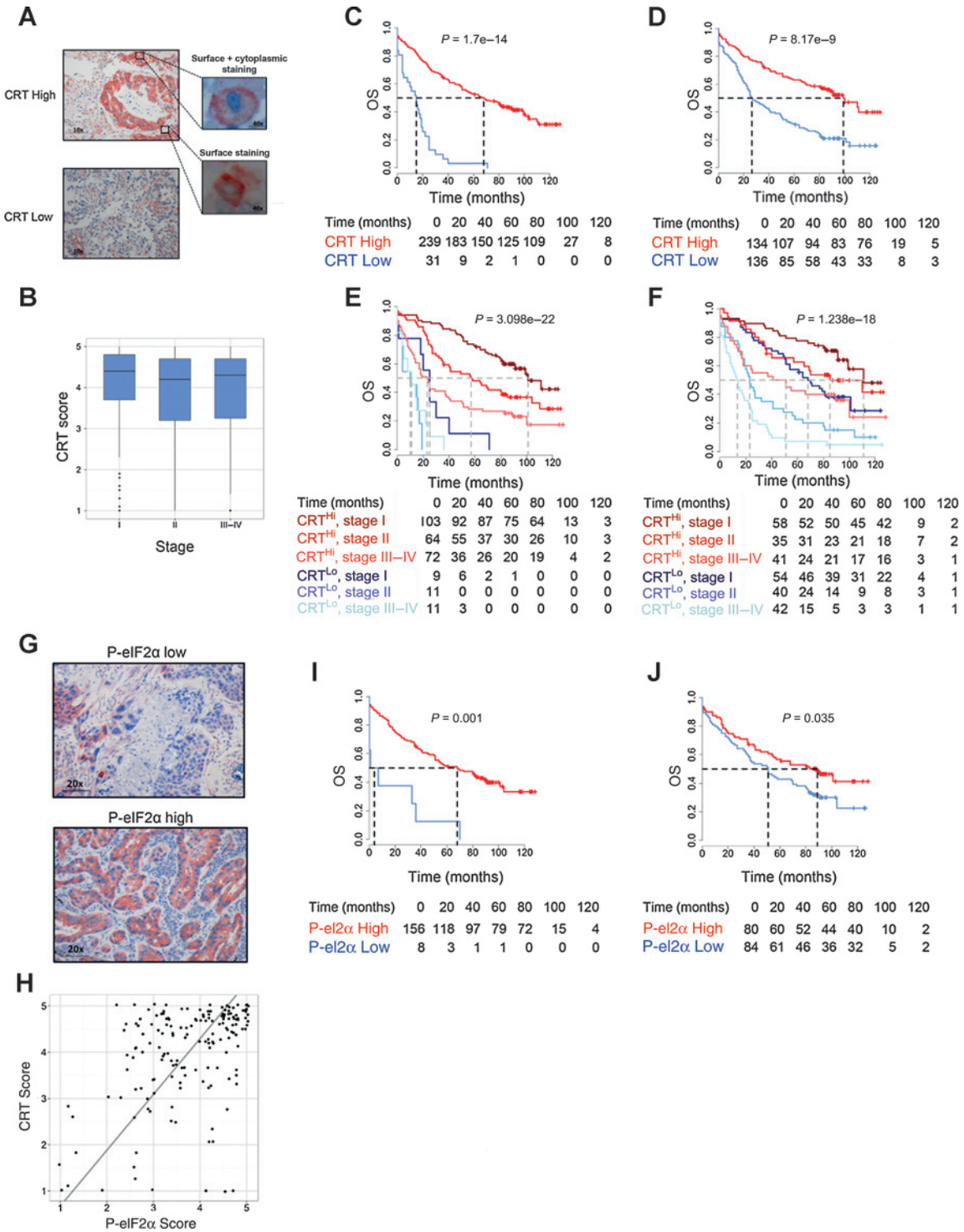

Figure 1.

Positive prognostic value conferred by tumoral CRT and P-eiF2α expression in NSCLC patients. Representative images showing low and high CRT expression in NSCLC tissue. A, CRT-positive cells are shown in red. B, boxplots representing the distributions of CRT score according to stages. Kaplan–Meier survival curves for OS for 270 patients with NSCLC without neoadjuvant chemotherapy according to the presence of a high or low expression of CRT evaluated using the optimal cut-off approach, $P = 1.7 \times 10^{-14}$ (C), using median, $P = 8.17 \times 10^{-9}$ (D) and using both CRT expression as well as stage stratification using the optimal cut-off approach, $P = 3.1 \times 10^{-22}$ (E) and using median, $P = 1.23 \times 10^{-18}$ (F). Representative images showing low and high P-eIF2α expression in NSCLC tissue. G, P-eIF2α–positive cells are shown in red. Correlation graph for P-eIF2α and CRT expression on tumor cells in the cohort of NSCLC patients. H, the gray line was determined by orthogonal regression. Kaplan–Meier survival curves for OS for 164 NSCLC patients according to the presence of a high or low density of P-eIF2α evaluated using optimal cut-off approach, $P = 0.0011$ (I) or using median, $P = 0.035$ (J). *P* value was determined by log-rank test. Tables show the number of patients at risk in each group at several time points.

Results

Prognostic impact of CRT expression in NSCLC

Tumor samples from a retrospective series of 270 patients with NSCLC (Table 1), who did not receive neoadjuvant chemotherapy, were analyzed for CRT expression by IHC (Fig. 1A). We observed a heterogeneous distribution of CRT expression among different patient's tumors, with a score ranging from grade 1 to 5 (1 for weak expression and 5 for strong expression). CRT was found both in the cytoplasm and at the surface of tumor cells (Fig. 1A). We did not find a significant difference of CRT expression between TNM stages (Fig. 1B). We divided the cohort into two groups, with high (CRT^{Hi}) and low (CRT^{Lo}) CRT expression on tumor cells, using the minimal *P* value approach (Fig. 1C). Calculations of the optimal cutoff [stratifying according to the minimization of the *P* value of a log-rank test, which was corrected using the method published by Altman and colleagues (37) to control for multiple testing] set the limit of the expression score at 2.45 (Supplementary Fig. S1A). This approach revealed that low CRT expression was associated to poor prognosis ($P = 1.7 \times 10^{-14}$) and allowed for the identification of a small group of patients with low CRT expression affected by a particularly short OS (Fig. 1C). The median OS was 18 months for the CRT^{Lo} group and 68 months for the CRT^{Hi} group. Univariate Cox modeling confirmed the prognostic impact of CRT quantification (Table 2, $P = 1.1 \times 10^{-16}$) and that CRT^{Lo} group of patients had a higher risk of death compared with CRT^{Hi} group ($P = 4.04 \times 10^{-14}$). However, as CRT^{Hi} and CRT^{Lo} groups of patients are disproportionate when using the optimal cutoff, we also used the median stratification, which confirmed that high CRT expression ($n = 134/270$) was strongly correlated with longer OS ($P = 8.17 \times 10^{-9}$; Fig. 1D). The median OS was 28 months for CRT^{Lo} group and increased to 100 months for the CRT^{Hi} group (Fig. 1D). Kaplan–Meier survival curves were also significantly different across quartiles of CRT expression, revealing a dose–effect relationship (Supplementary Fig. S2; $P = 4.35 \times 10^{-12}$). These results define CRT expression as a strong predictive marker for OS of NSCLC patients.

As CRT expression did not correlate with pathologic staging (Fig. 1B), the current gold standard for lung cancer risk assessment, we investigated whether these two parameters are independently prognostic, by using a multivariate Cox model (Table 3). CRT expression, pathologic staging, and age turned out to be the only significant predictors of OS. Kaplan–Meier curves combining stage and CRT stratifications using the optimal *P* value (Fig. 1E) and median cutoffs (Fig. 1F) were consistent with this interpretation. CRT^{Hi}/stage I patients had the best OS prognosis (median OS was 101 or 110 months using optimal or median cutoff, respectively). In contrast, patients in the pathologic stage III–IV and low expression of CRT were at the highest risk of death (median OS was 11 or 14 months using optimal or median stratification, respectively; Fig. 1E and F). Of note, when the optimal cutoff for stratifying tumors into CRT^{Lo} and CRT^{Hi} is used, it appears that CRT^{Lo}/stage I patients succumb more quickly than CRT^{Hi}/stage III–IV patients (Fig. 1E), suggesting that CRT low expression can identify patients with high risk of death even at early stages. Altogether, these data show that CRT expression and pathologic stage are independent prognostic factors.

Table 2. Univariate Cox regression for patients without neoadjuvant chemotherapy

Variable	HR (95% CI)	*P*
Sex (F vs. M)	1.25 (0.83–1.91)	0.28
Age, years	1.02 (1.0–1.036)	**0.004**
Smoking history		
Never smoker vs. smoker	0.78 (0.47–1.27)	0.32
Histologic type		
ADC vs. SCC	1.18 (0.85–1.63)	0.31
ADC vs. others	1.26 (0.65–2.42)	0.49
Stage		
I vs. II	1.87 (1.28–2.73)	**0.001**
I vs. III–IV	2.99 (2.08–4.30)	**2.7e−09**
CRT score	0.54 (0.47–0.61)	**1.10e−16**
P-eiF2α score	0.72 (0.58–0.89)	**0.003**
Log_{10} DC-LAMP density	0.72 (0.56–0.93)	**0.01**
Log_{10} CD8 density	0.67 (0.56–0.80)	**1.87e−5**
CRT group, Hi vs. Low	4.98 (3.28–7.55)	**4.04e−14**

NOTE: Univariate Cox proportional hazards analysis for OS according to clinical and immune parameters. Bold, $P < 0.05$.
Abbreviations: ADC, adenocarcinoma; SCC, squamous cell carcinoma.

We performed CRT quantification as well as survival analyzes in an independent cohort of 125 patients that were all affected by stage III NSCLC and treated with neoadjuvant chemotherapy (Supplementary Table S2). These patients received platinum salt-based chemotherapy in combination with gemcitabine (46%), vironelbine (34%), paclitaxel (14%), or anthracyclines (6%) before surgery. Again, expression of CRT using the optimal *P* value approach confirmed a strong prognostic impact of the CRT-based stratification (Supplementary Fig. S3A, $P = 0.017$), and CRT expression below the median level was also associated with poor prognosis (Supplementary Fig. S3B, $P = 0.0074$). Univariate Cox analysis confirmed the prognostic impact of CRT expression in this cohort of patients (HR = 0.78, $P = 0.0045$; Supplementary Table S3).

The comparison of CRT expression level by tumor cells between the two cohorts of patients revealed no differences (Supplementary Fig. S4A), indicating that the received neoadjuvant chemotherapy did not influence CRT expression.

Correlation between eIF2α phosphorylation and CRT expression in lung tumor cells

The translocation of CRT to the cell surface is triggered in response to an ER stress that involves the phosphorylation of the eukaryotic translation initiation factor eIF2α by PKR-like ER kinase (PERK; refs. 19, 23, 38). Using IHC, we found that phosphorylated-eIF2α (P-eIF2α) was mostly expressed in NSCLC cells (as opposed to stromal elements), although with an interindividual variability, similarly to that found for CRT staining (Fig. 1G). We observed a statistically significant correlation between the expression of P-eIF2α and CRT in the two cohorts of NSCLC patients that were either not treated ($P = 2.7 \times 10^{-10}$, r = 0.46, Fig. 1H) or treated with neoadjuvant chemotherapy ($P = 2.3 \times 10^{-13}$, $r = 0.70$, Supplementary Fig. S3E). High P-eiF2α expression was correlated with longer survival using optimal cutoff ($P = 0.001$; Fig. 1I and $P = 0.0033$ Supplementary Fig. S3C, respectively for the cohorts of patients that were not treated and treated with neoadjuvant chemotherapy), and using median stratification ($P = 0.0035$ Fig. 1J and $P = 0.0333$ Supplementary Fig. S3D,

Table 3. Multivariate Cox regression for patients without neoadjuvant chemotherapy

Variable	HR (95% CI)	*P*
Age, years	1.02 (1.00–1.05)	**0.027**
Stage		
I vs. II	1.93 (1.14–3.27)	**0.013**
I vs. III–IV	2.21 (1.31–3.73)	**0.002**
CRT score	0.59 (0.47–0.73)	**1.91e−06**
P-eiF2α score	0.91 (0.71–1.15)	0.44
Log_{10} DC-LAMP density	1.00 (0.72–1.40)	0.99
Log_{10} CD8 density	0.86 (0.64–1.15)	0.31

NOTE: Multivariate Cox proportional hazards analyses for OS according to clinical and immune parameters. Parameters identified in the univariate analysis as significantly influencing outcome were introduced in a multivariate Cox proportional hazards regression model. Bold, $P < 0.05$.

respectively, for the cohorts of patients that were not treated and treated with neoadjuvant chemotherapy). We did not observe any difference in the distribution of P-eiF2α between untreated and neoadjuvant-treated patients (Supplementary Fig. S4B), indicating that the neoadjuvant chemotherapy did not effect on P-eiF2α phosphorylation.

For both cohorts, univariate Cox analysis revealed that CRT and P-eIF2α were significantly associated to OS (Table 2 and Supplementary Table S3). We analyzed the prognostic value of the two parameters using multivariate Cox proportional hazards regression (Table 3 and Supplementary Table S4). P-eIF2α then lost its prognostic impact, which indicates that the strong correlation between the two variables prevents their concomitant use for risk assessment.

High expression of CRT is associated with an enhanced cellular immune response

CRT is best characterized for its prominent function as an eat-me signal, leading to maturation of DCs and activation of adaptive immune responses against tumors (39). Therefore, we addressed the impact of CRT expression on the density of tumor-infiltrating immune cells, including mature DCs (DC-LAMP$^+$ cells, Fig. 2A), CD8$^+$ T cells (Fig. 2B), CD8/KI67 proliferating CD8$^+$ T cells, CD20$^+$ B cells, and CD68$^+$ macrophages (data not shown and Supplementary Fig. S5), in the cohort of untreated patients. The great majority of the samples contained rather low numbers of DC-LAMP$^+$ cells, mainly found in the tumor stroma and associated with the tertiary lymphoid structures, as we previously reported (8). Patients with high CRT expression exhibited significantly ($P = 0.042$) higher densities of mature DCs (medians 1.1 and 0.6 cells/mm^2 for CRT^{Hi} and CRT^{Lo} groups respectively, Fig. 2A). However, there was no significant difference in the CD8$^+$ T-cell density ($P = 0.15$; Fig. 2B), B-cell density ($P = 0.27$), macrophage density ($P = 0.92$; Supplementary Fig. S5A), and in the number of CD8$^+$/Ki67$^+$ proliferating T cells ($P = 0.29$; Supplementary Fig. S5B), between CRT^{Hi} and CRT^{Lo} tumors. We also quantified the level of MHC-I expression by tumor cells and found that MHC-I expression was highly heterogeneous among patients. There was no difference in MHC-I expression between CRT^{Hi} and CRT^{Lo} tumors ($P = 0.7$; Supplementary Fig. S5C).

Confirming prior observations (9), high densities of DC-LAMP$^+$ cells, and of CD8$^+$ T cells had a positive impact on patient survival (Supplementary Fig. S6A and S6B). Univariate Cox

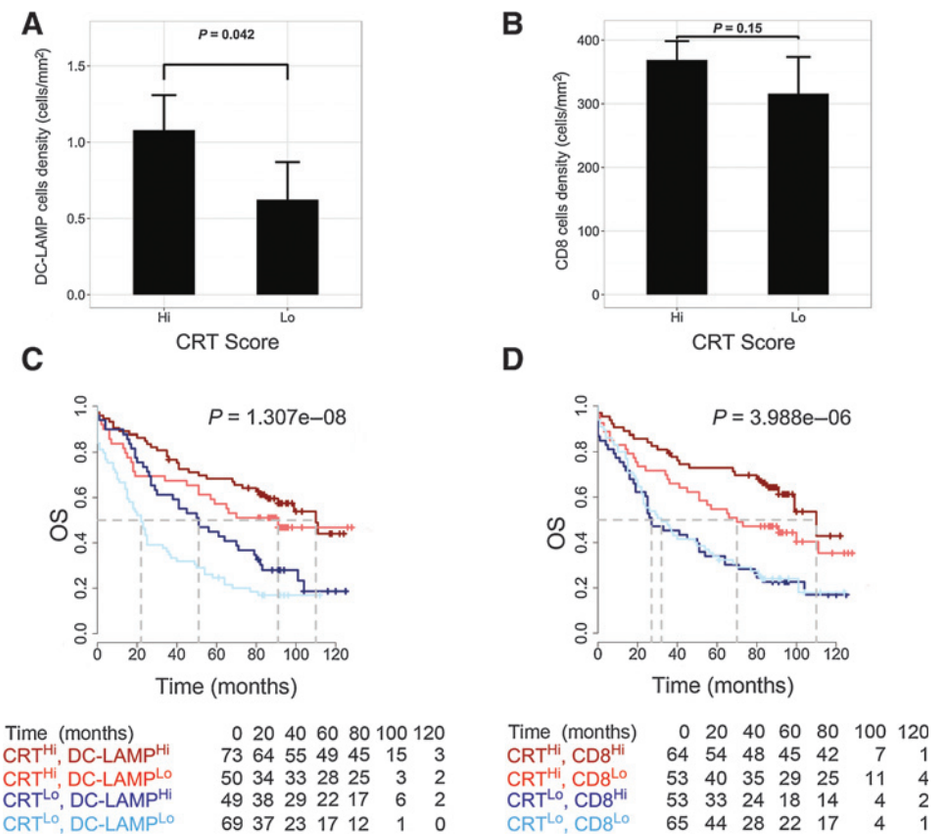

Time (months)	0	20	40	60	80	100	120
CRT^{Hi}, DC-LAMP^{Hi}	73	64	55	49	45	15	3
CRT^{Hi}, DC-LAMP^{Lo}	50	34	33	28	25	3	2
CRT^{Lo}, DC-LAMP^{Hi}	49	38	29	22	17	6	2
CRT^{Lo}, DC-LAMP^{Lo}	69	37	23	17	12	1	0

Time (months)	0	20	40	60	80	100	120
CRT^{Hi}, CD8^{Hi}	64	54	48	45	42	7	1
CRT^{Hi}, CD8^{Lo}	53	40	35	29	25	11	4
CRT^{Lo}, CD8^{Hi}	53	33	24	18	14	4	2
CRT^{Lo}, CD8^{Lo}	65	44	28	22	17	4	1

Figure 2.
Prognostic value conferred by tumor CRT expression combined with DC-LAMP and CD8 densities in NSCLC patients. Barplots representing the median DC-LAMP$^+$ (A) and CD8$^+$ T-cell densities (B) in CRT^{Hi} and CRT^{Lo} groups. Kaplan–Meier survival curves for OS for NSCLC patients according CRT expression combined with the presence of a high or low density of DC-LAMP$^+$ cells, $P = 1.3 \times 10^{-8}$ (C), or CD8$^+$ T cells, $P = 3.98 \times 10^{-6}$ (D), evaluated using the median cut-off approach. *P* value was determined by the log-rank test. Tables show the number of patients according to the expression of CRT and DC-LAMP or CD8 high and low groups.

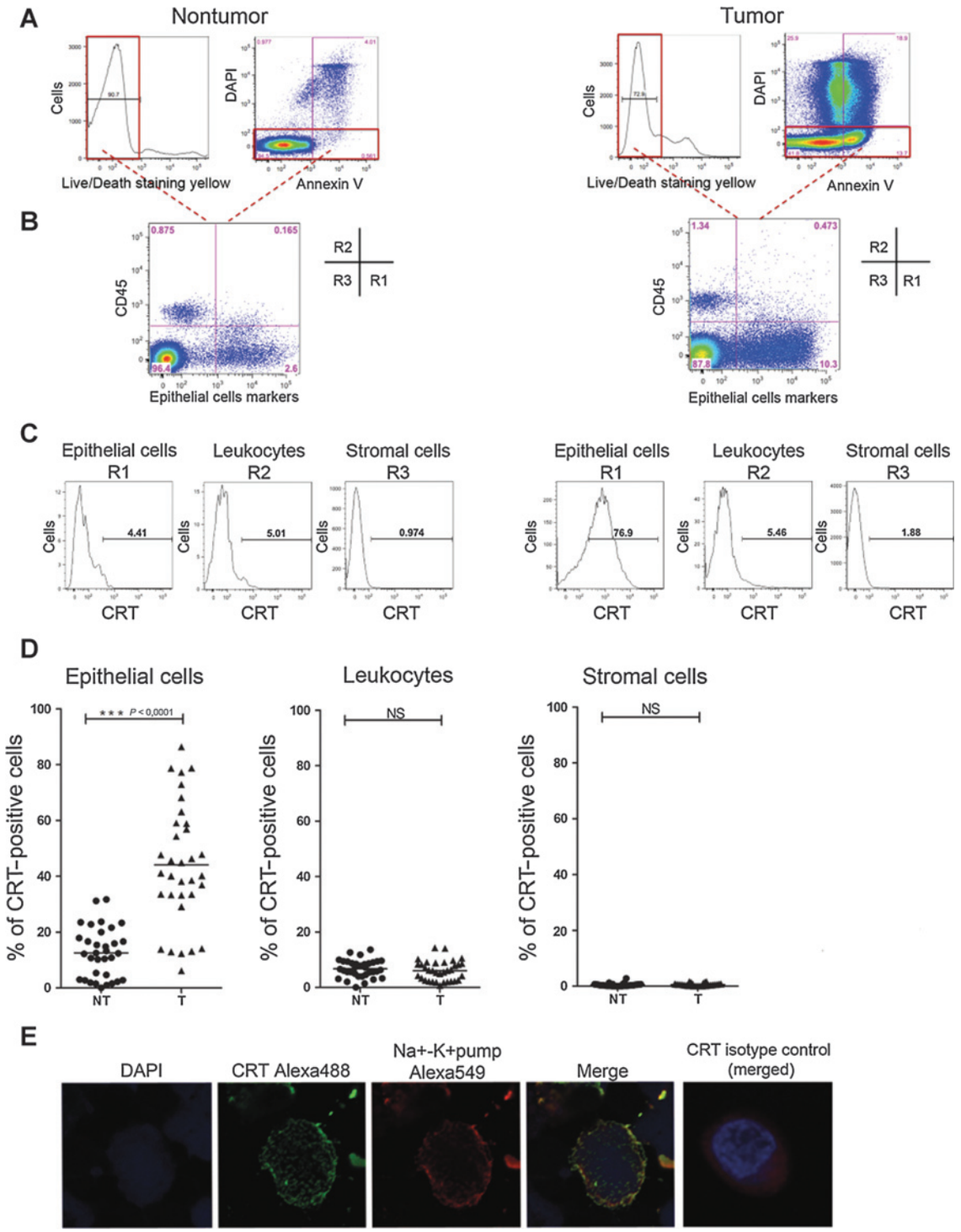

Figure 3.
Primary epithelial cells of NSCLC patients can expose CRT at their cell surface. Flow cytometry analysis of CRT expression on the cell surface of epithelial cells, leukocytes, and stromal cells. Histograms representing strategy of gating for nontumoral (left) and tumoral tissues (right) among NSCLC patients treated by primary surgery. A, only DAPI$^-$ cells or Live/Death staining yellow–negative cells were selected for further analysis of CD45$^+$ and cells positive for epithelial markers (EM). B, cells located in top left quadrant CD45$^+$/EM$^-$ (R2) represent the population of leukocytes, cells located in lower left quadrant CD45$^-$/EM$^-$ (R3) represent the population of stromal cells, and cells located in bottom right quadrant CD45$^-$/EM$^+$ (R1) represent the population of epithelial cells. C, representative histograms for cell surface expression of CRT determined by cytometry on epithelial cells, leukocytes, and stromal cells in both nontumoral (left) and tumoral tissues (right panel). D, CRT surface expression on epithelial cells, leukocytes, and stromal cells in nontumoral (NT) or tumoral tissues (T) in a cohort of 50 NSCLC patients. *P* values were calculated by *t*-test; ***, $P < 0.001$. E, representative confocal microscopy staining for CRT on the cell surface that colocalized with Na$^+$-K$^+$ pump surface staining. *P* values were calculated by *t* test, NS, nonsignificant.

analysis confirmed the prognostic value of mature DC and $CD8^+$ T-cell densities (Table 2).

We evaluated the combined prognostic value of CRT plus DC-LAMP or CD8, at the median cutoff (Fig. 2C and D). We observed that CRT^{Hi} patients had the best OS whatever the level of DC-LAMP. CRT^{Hi}/DC-$LAMP^{Hi}$ group had the best prognosis (median OS = 110 months) compared with patients with CRT^{Hi}/DC-$LAMP^{Lo}$, which were at an intermediate risk of death (median OS = 92 months). The CRT^{Lo}/DC-$LAMP^{Lo}$ group of patients was at the highest risk of death (median OS was 21 months; Fig. 2C). The combination of CRT expression and CD8 density yielded similar results, with the best prognosis for CRT^{Hi}/$CD8^{Hi}$ patients, intermediate values for CRT^{Hi}/$CD8^{Lo}$ tumors, and dismal prognosis for CRT^{Lo}/$CD8^{Lo}$ and CRT^{Lo}/$CD8^{Hi}$ groups (Fig. 2D). Similar results were obtained when using the optimal cutoff for CRT score (Supplementary Fig. S6C and S6D).

Using multivariate Cox analysis, the age, the pTNM stage, and the CRT score were found to be significantly and independently associated with OS, whereas mature DC and CD8 cell densities were not found significantly associated with OS (Table 3). Altogether, these data demonstrate that CRT expression and mature DC or $CD8^+$ T-cell densities are not independent prognostic factors.

Cell surface exposure of CRT on primary tumor cells from NSCLC patients

By using IHC, the exposure of CRT expression at the cell surface of tumor cells is not easily quantifiable. We performed flow cytometry analysis on freshly resected human NSCLC patients treated by primary surgery to characterize the expression of CRT (Fig. 3). Surface CRT expression was detected in the population of $AnnexinV^{+/-}$/$DAPI^-$ cells (or alternatively live cells detected by a Live/Death Staining Kit) in nontumoral and in tumoral tissues (Fig. 3A). Using an antibody against the leukocyte marker CD45 and a panel of antibodies specific for epithelial surface markers, we distinguished populations of leukocytes, stromal, and epithelial cells (Fig. 3B). The percentage of CRT-positive cells was evaluated among these cells in both tumoral and distant nontumoral tissues (Fig. 3C and D). Although highly heterogeneous, the expression of membrane CRT was significantly increased ($P < 0.0001$) on tumor epithelial cells as compared with epithelial cells from nontumoral tissues in the majority of patients (Fig. 3D). Leukocytes and stromal cells from tumoral and nontumoral tissues did not express CRT on their surface (Fig. 3D), although such cells did contain intracellular CRT, as revealed by immunofluorescence staining after plasma membrane permeabilization (Supplementary Fig. S7) using a similar gating strategy. Confocal microscopy of epithelial tumor cells stained for ecto-CRT and the Na^+-K^+ pump confirmed that CRT was indeed localized at the plasma membrane of the majority of the tumor cells (Fig. 3E).

Because the expression of CRT can strongly influence the population of immune cells, we evaluated the impact of membrane CRT expression by tumor cells, on the immune cell infiltrate with a focus on T lymphocytes and DCs [$CD45^+$, $CD3^+$, $CD4^+$, $CD8^+$, plasmacytoid DCs (pDC) and myeloid DCs (cDC; Fig. 4A)]. We observed a significant lower percentage of total $CD45^+$ and $CD4^+$ cells and a significantly higher percentage of cDCs in CRT^{high}, patients, compared with CRT^{low} patients, among total live mononuclear cells from the tumor. Furthermore, we determined the frequency of the four main subpopulations of $CD4^+$ and $CD8^+$ T cells, related to their differentiation status. As compared with CRT^{low} tumors, CRT^{high} tumors were significantly more infiltrated by $CD4^+$ and $CD8^+$ effector memory T cells ($CD45RA^-$/$CCR7^-$; Fig. 4B), whereas the percentage of naïve and terminally differentiated effector-memory (also called TEM-RA) $CD4^+$ and $CD8^+$ T cells was significantly decreased ($P < 0.05$). No difference was seen for central memory $CD4^+$ and $CD8^+$ T cells. Altogether, these results demonstrate that CRT^{high} tumors have higher percentages of activated and effector-memory T cells than CRT^{low} tumors.

Discussion

CRT has been evaluated as a potential biomarker in several types of cancer including neuroblastoma (40), bladder (41), gastric (42), breast cancer (43), and acute myeloid leukemia (38). CRT has also been reported to be overexpressed in the cytoplasm and at the membrane level of NSCLC cells, and serum level of CRT protein was associated with tumor pathologic grade (44), although the prognostic impact of circulating CRT levels has not been studied. Here, we assessed the prognostic value of CRT expression in two independent retrospective cohorts of patients with NSCLC, one treated by primary surgery without neoadjuvant chemotherapy ($n = 270$, stage I to III–IV) and the second one treated by neoadjuvant chemotherapy followed by surgery ($n = 125$, stage III N2).

In NSCLC samples, we observed a major interindividual variability in CRT expression irrespective of the histologic subtype of NSCLC. Nevertheless CRT expression was not affected by the stage and Cox multivariate regression analyses confirmed that CRT expression and stage are two independent prognostic factors. High levels of CRT were associated with long survival of NSCLC patients. Our data are in accordance with findings in neuroblastoma (40), in which high CRT correlates with neuroblastoma differentiation and favorable outcome. Conversely, in esophageal squamous cell carcinoma, CRT expression had no impact on patients' survival (32), suggesting that CRT levels may only predict patient survival in some cancer types. In our study, CRT expression strongly correlated with the constitutive phosphorylation of eIF2α. This suggests that a subgroup of NSCLC is associated with a strong constitutive ER stress response that culminates in CRT expression and exposure, facilitating anticancer immunosurveillance. To date, the precise mechanisms that explain why some but not all NSCLCs are inclined to ER stress and others not remain to be elucidated. In breast cancer, changes in ploidy have been linked to the level of eIF2α phosphorylation and the intensity of the tumor infiltrate after anthracycline-based chemotherapy (45). Whether similar mechanisms apply to NSCLC remains to be investigated.

We observed similar levels of CRT and P-eiF2α expression by tumor cells from patients that were left untreated or underwent neoadjuvant chemotherapy. Similar results were obtained in the prospective cohorts of patients, in which we demonstrated high expression of CRT at the cell surface of tumor cells in some patients. In addition, high CRT and P-eiF2α expression conferred a good clinical outcome in both cohorts. These results demonstrate that received chemotherapy is not the driver for high CRT expression or for CRT exposure at the cell surface, in

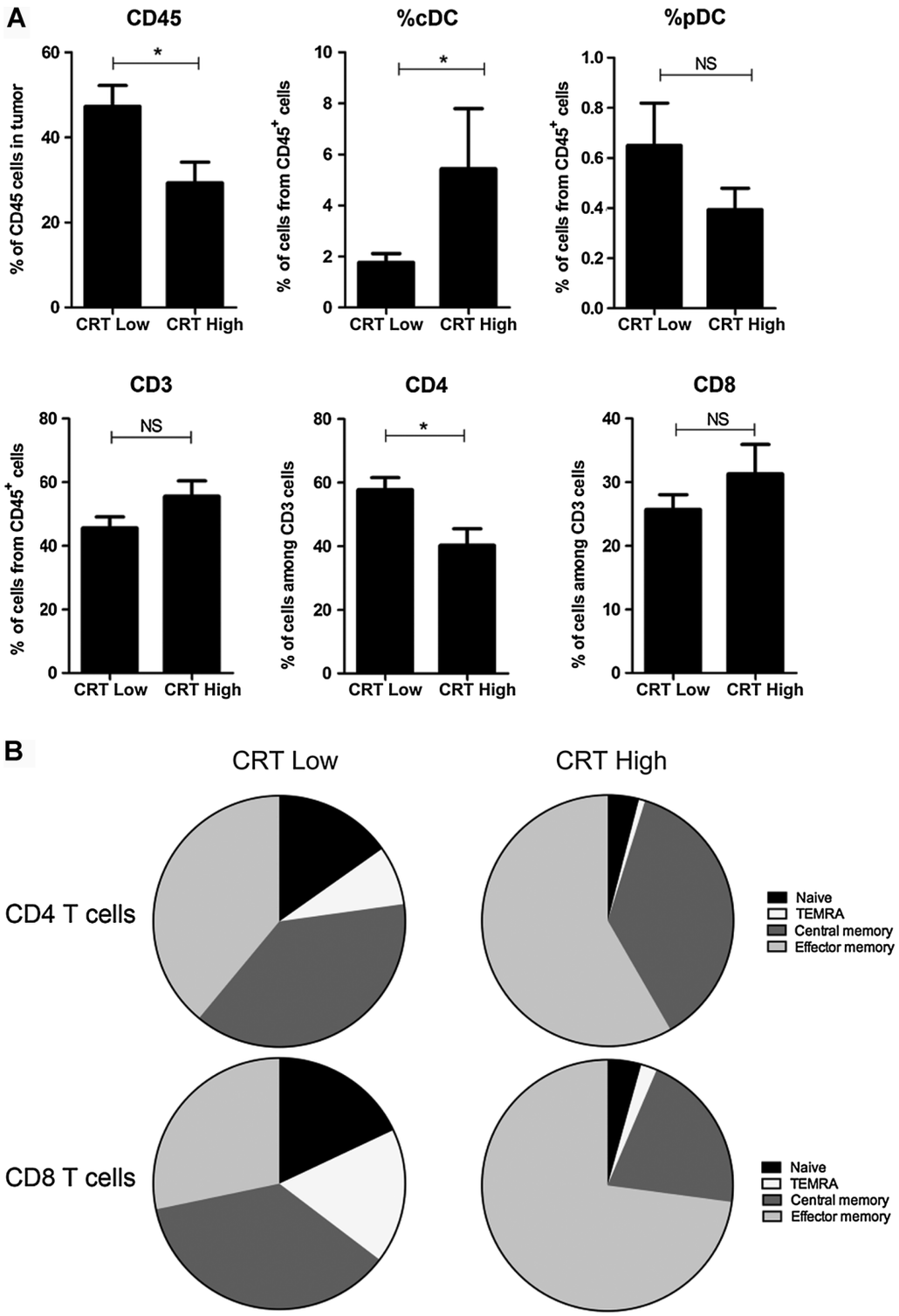

Figure 4.
Phenotypic analysis of the immune cell infiltrate according to the high and low expression of CRT among prospective cohort of NSCLC patients. Large-scale flow cytometry analysis of immune cell populations stratified by the expression of CRT in 25 fresh lung tumors (13 CRT^{low} tumors vs. 12 CRT^{high} tumors using median stratification). Expression of CRT was evaluated by flow cytometry. A, the percentage of different cell types among total live mononuclear cells from the tumors of CRT^{high} and CRT^{low} is shown. The percentage of total CD45, myeloid (cDC), and plasmacytoid dendritic (pDC) cells defined as $CD45^+$ $CD3^-$ $CD16^-$ $CD19^-$ $CD14^-$ HLA-DR^+ $CD11c^+$ and $CD45^+$ $CD3^-$ $CD16^-$ $CD19^-$ $CD14^-$ HLA-DR^+ $CD123^+$, respectively (cDCs and pDCs) and CD3 T cells and CD4 and CD8 T-cell subsets is shown. B, percentages of T-cell subsets with naïve, effector memory, central memory and terminally differentiated effector memory (TEM-RA) phenotype, based on expression of CD45RA and CCR7, in CRT^{high} and CRT^{low} tumors are shown. *P* values were calculated by *t* test; *, $P < 0.05$.

line with similar findings reported by by Wemeau and colleagues in the context of acute myeloid leukemia patients (38).

When present at the surface of tumor cells, CRT can stimulate antigen-presenting cells, particularly DCs, to efficiently engulf dying cells, process their antigens and prime T-cell immune response (16, 19, 29). Accordingly, a high density of mature DCs closely correlated with high expression of CRT in NSCLC. Previous reports demonstrated that high levels of ecto-CRT on tumor cells positively correlated with the activation of DCs and the capacity of DCs to stimulate IFNγ by autologous T cells (17, 19, 29). However, we did not observe a major positive correlation between the density of total $CD8^+$ T cells and CRT expression in NSCLC. In a cohort of prospective patients treated by primary surgery without neoadjuvant chemotherapy, we have observed significantly higher percentage of cDCs and effector memory $CD4^+$ and $CD8^+$ T cells in CRT^{high} tumors than in CRT^{low} NSCLCs, whereas the frequency of total $CD4^+$ and $CD8^+$ T cells was identical. These data are in accordance with results showing that the densities of infiltrating mature DC and effector-memory T cells correlate among each other (9). These results demonstrate that high CRT expression at the cell surface of tumor cells leads to elevated frequency of mature DCs, and impact the quality of antitumor immune response, leading to the differentiation of tumor-infiltrating T cells towards an effector memory phenotype. Effector-memory T cells have been identified to control cancer progression. Mainly the cytotoxic and cytokinic capability of effector memory T cells may provide them the relevant weapons to control tumor progression and metastatic invasion at the primary tumor site (46). In numerous cancers, the presence of tumor-infiltrating effector memory T cells correlates with reduced metastatic invasion and increased survival of the patient (47). When looking at other effectors of the immune response, we did not find any difference in the density of tumor-infiltrating B cells and macrophages. In addition, because CRT is an ER-chaperone molecule, its expression level might affect the loading of peptide on MHC-I, and hence the level of MHC-I expression at the cell surface. However, we did not find any difference in the expression level of MHC-I molecules on cancer cells from CRT^{Hi} and CRT^{Lo} patients.

The most favorable prognosis was observed for the group of patients with high CRT expression and high density of $DC\text{-}LAMP^+$ or $CD8^+$ cells. Patients with high CRT and low $DC\text{-}LAMP^+$ or $CD8^+$ cells were at an intermediate risk. Individuals with low expression of CRT in their NSCLC were at the highest risk of death, irrespective of the density of DC or $CD8^+$ T cells in the tumor infiltrate. This points to the possibility that the immune reaction in CRT^{Hi} tumors may be particularly active in anticancer immunosurveillance, probably involving ICD leading to an effective $CD8^+$ T-cell response directed against tumor-associated antigens, while that of CRT^{Lo} tumors would be dysfunctional. In this case, one could speculate that in the absence of efficacious priming, the T-cell response is polyclonal and not efficient. However, this conjecture requires further experimental exploration.

In conclusion, high CRT expression, which is likely driven by an ER stress response, constitutes a positive prognostic biomarker in NSCLC patients. The available data are compatible with the hypothesis that the local presence of CRT, which is constitutively expressed at the surface of transformed epithelial cells, may enable DC-dependent anticancer immunosurveillance.

Disclosure of Potential Conflicts of Interest

E. Becht is a consultant/advisory board member for SOTIO. W.-H. Fridman is a consultant/advisory board for LFB, Sanofi, and Servier. No potential conflicts of interest were disclosed by the other authors..

Authors' Contributions

Conception and design: J. Fucikova, G. Kroemer, C. Sautes-Fridman, I. Cremer
Development of methodology: J. Fucikova, J. Goc, P. Devi, M.-C. Dieu-Nosjean
Acquisition of data (provided animals, acquired and managed patients, provided facilities, etc.): J. Fucikova, J. Goc, R. Remark, D. Damotte, M. Alifano, P. Devi, J. Biton, A. Lupo, C. Germain, M.-C. Dieu-Nosjean
Analysis and interpretation of data (e.g., statistical analysis, biostatistics, computational analysis): J. Fucikova, E. Becht, J. Goc, R. Remark, D. Damotte, P. Devi, W.-H. Fridman, M.-C. Dieu-Nosjean, I. Cremer
Writing, review, and/or revision of the manuscript: J. Fucikova, E. Becht, J. Goc, P. Devi, C. Germain, W.-H. Fridman, M.-C. Dieu-Nosjean, G. Kroemer, C. Sautes-Fridman, I. Cremer
Administrative, technical, or material support (i.e., reporting or organizing data, constructing databases): J. Fucikova, K. Iribarren, A. Lupo
Study supervision: I. Cremer

Grant Support

This work was supported by the "Institut National de la Santé et de la Recherche Médicale" (INSERM), Université Pierre et Marie Curie, Université Paris Descartes, the Cancer Research for Personalized Medicine (CARPEM), the Paris Alliance of Cancer Research Institutes (PACRI), the LabEx Immuno-Oncology, and the Institut National du Cancer (2011-PLBIO-06-INSERM 6-1, PLBIO09-088-IDF-KROEMER. J. Fucikova was supported by grant IGA NT 14533 and IGA NT 11404-5, Ministry of Health, Czech Republic.

The costs of publication of this article were defrayed in part by the payment of page charges. This article must therefore be hereby marked *advertisement* in accordance with 18 U.S.C. Section 1734 solely to indicate this fact.

Received April 28, 2015; revised November 17, 2015; accepted December 11, 2015; published OnlineFirst February 3, 2016.

References

1. Mittal D, Gubin MM, Schreiber RD, Smyth MJ. New insights into cancer immunoediting and its three component phases–elimination, equilibrium and escape. Curr Opin Immunol 2014;27:16–25.
2. Vesely MD, Kershaw MH, Schreiber RD, Smyth MJ. Natural innate and adaptive immunity to cancer. Annu Rev Immunol 2011;29:235–71.
3. Fridman WH, Pages F, Sautes-Fridman C, Galon J. The immune contexture in human tumours: impact on clinical outcome. Nat Rev Cancer 2012;12:298–306.
4. Galon J, Costes A, Sanchez-Cabo F, Kirilovsky A, Mlecnik B, Lagorce-Pages C, et al. Type, density, and location of immune cells within human colorectal tumors predict clinical outcome. Science 2006;313:1960–4.
5. Sautes-Fridman C, Cherfils-Vicini J, Damotte D, Fisson S, Fridman WH, Cremer I, et al. Tumor microenvironment is multifaceted. Cancer Metastasis Rev 2011;30:13–25.
6. Fialova A, Partlova S, Sojka L, Hromadkova H, Brtnicky T, Fucikova J, et al. Dynamics of T-cell infiltration during the course of ovarian cancer: the gradual shift from a Th17 effector cell response to a predominant infiltration by regulatory T-cells. Int J Cancer 2013;132:1070–9.
7. Mlecnik B, Tosolini M, Kirilovsky A, Berger A, Bindea G, Meatchi T, et al. Histopathologic-based prognostic factors of colorectal cancers are associated with the state of the local immune reaction. J Clin Oncol 2011;29:610–8.
8. Dieu-Nosjean MC, Antoine M, Danel C, Heudes D, Wislez M, Poulot V, et al. Long-term survival for patients with non-small-cell lung cancer with intratumoral lymphoid structures. J Clin Oncol 2008;26:4410–7.
9. Goc J, Germain C, Vo-Bourgais TK, Lupo A, Klein C, Knockaert S, et al. Dendritic cells in tumor-associated tertiary lymphoid structures

signal a Th1 cytotoxic immune contexture and license the positive prognostic value of infiltrating CD8+ T cells. Cancer Res 2014; 74:705–15.
10. Becht E, Goc J, Germain C, Giraldo NA, Dieu-Nosjean MC, Sautes-Fridman C, et al. Shaping of an effective immune microenvironment to and by cancer cells. Cancer Immunol Immunother 2014;63:991–7.
11. Kroemer G, Galluzzi L, Kepp O, Zitvogel L. Immunogenic cell death in cancer therapy. Annu Rev Immunol 2013;31:51–72.
12. Vacchelli E, Senovilla L, Eggermont A, Fridman WH, Galon J, Zitvogel L, et al. Trial watch: Chemotherapy with immunogenic cell death inducers. Oncoimmunology 2013;2:e23510.
13. Garg AD, Dudek AM, Agostinis P. Cancer immunogenicity, danger signals, and DAMPs: what, when, and how? BioFactors 2013;39:355–67.
14. Dudek AM, Garg AD, Krysko DV, De Ruysscher D, Agostinis P. Inducers of immunogenic cancer cell death. Cytokine Growth Factor Rev 2013; 24:319–33.
15. Obeid M, Tesniere A, Ghiringhelli F, Fimia GM, Apetoh L, Perfettini JL, et al. Calreticulin exposure dictates the immunogenicity of cancer cell death. Nat Med 2007;13:54–61.
16. Fucikova J, Kralikova P, Fialova A, Brtnicky T, Rob L, Bartunkova J, et al. Human tumor cells killed by anthracyclines induce a tumor-specific immune response. Cancer Res 2011;71:4821–33.
17. Spisek R, Charalambous A, Mazumder A, Vesole DH, Jagannath S, Dhodapkar MV. Bortezomib enhances dendritic cell (DC)-mediated induction of immunity to human myeloma via exposure of cell surface heat shock protein 90 on dying tumor cells: therapeutic implications. Blood 2007; 109:4839–45.
18. Martins I, Wang Y, Michaud M, Ma Y, Sukkurwala AQ, Shen S, et al. Molecular mechanisms of ATP secretion during immunogenic cell death. Cell Death Differ 2014;21:79–91.
19. Garg AD, Krysko DV, Verfaillie T, Kaczmarek A, Ferreira GB, Marysael T, et al. A novel pathway combining calreticulin exposure and ATP secretion in immunogenic cancer cell death. EMBO J 2012;31:1062–79.
20. Apetoh L, Ghiringhelli F, Tesniere A, Obeid M, Ortiz C, Criollo A, et al. Toll-like receptor 4-dependent contribution of the immune system to anticancer chemotherapy and radiotherapy. Nat Med 2007;13:1050–9.
21. Scaffidi P, Misteli T, Bianchi ME. Release of chromatin protein HMGB1 by necrotic cells triggers inflammation. Nature 2002;418:191–5.
22. Gardai SJ, McPhillips KA, Frasch SC, Janssen WJ, Starefeldt A, Murphy-Ullrich JE, et al. Cell-surface calreticulin initiates clearance of viable or apoptotic cells through trans-activation of LRP on the phagocyte. Cell 2005;123:321–34.
23. Panaretakis T, Kepp O, Brockmeier U, Tesniere A, Bjorklund AC, Chapman DC, et al. Mechanisms of pre-apoptotic calreticulin exposure in immunogenic cell death. EMBO J 2009;28:578–90.
24. Obeid M, Panaretakis T, Joza N, Tufi R, Tesniere A, van Endert P, et al. Calreticulin exposure is required for the immunogenicity of gamma-irradiation and UVC light-induced apoptosis. Cell Death Differ 2007; 14:1848–50.
25. Ghiringhelli F, Apetoh L, Tesniere A, Aymeric L, Ma Y, Ortiz C, et al. Activation of the NLRP3 inflammasome in dendritic cells induces IL-1beta-dependent adaptive immunity against tumors. Nat Med 2009;15:1170–8.
26. Tesniere A, Schlemmer F, Boige V, Kepp O, Martins I, Ghiringhelli F, et al. Immunogenic death of colon cancer cells treated with oxaliplatin. Oncogene 2010;29:482–91.
27. Menger L, Vacchelli E, Adjemian S, Martins I, Ma Y, Shen S, et al. Cardiac glycosides exert anticancer effects by inducing immunogenic cell death. Sci Transl Med 2012;4:143ra99.
28. Chen HM, Wang PH, Chen SS, Wen CC, Chen YH, Yang WC, et al. Shikonin induces immunogenic cell death in tumor cells and enhances dendritic cell-based cancer vaccine. Cancer Immunol Immunother 2012;61:1989–2002.
29. Fucikova J, Moserova I, Truxova I, Hermanova I, Vancurova I, Partlova S, et al. High hydrostatic pressure induces immunogenic cell death in human tumor cells. Int J Cancer 2014;135:1165–77.
30. Miyamoto S, Inoue H, Nakamura T, Yamada M, Sakamoto C, Urata Y, et al. Coxsackievirus B3 is an oncolytic virus with immunostimulatory properties that is active against lung adenocarcinoma. Cancer Res 2012;72:2609–21.
31. Brusa D, Garetto S, Chiorino G, Scatolini M, Migliore E, Camussi G, et al. Post-apoptotic tumors are more palatable to dendritic cells and enhance their antigen cross-presentation activity. Vaccine 2008; 26:6422–32.
32. Suzuki Y, Mimura K, Yoshimoto Y, Watanabe M, Ohkubo Y, Izawa S, et al. Immunogenic tumor cell death induced by chemoradiotherapy in patients with esophageal squamous cell carcinoma. Cancer Res 2012;72:3967–76.
33. Stangl S, Themelis G, Friedrich L, Ntziachristos V, Sarantopoulos A, Molls M, et al. Detection of irradiation-induced, membrane heat shock protein 70 (Hsp70) in mouse tumors using Hsp70 Fab fragment. Radiother Oncol 2011;99:313–6.
34. Detterbeck FC, Boffa DJ, Tanoue LT. The new lung cancer staging system. Chest 2009;136:260–71.
35. Brambilla E, Travis WD, Colby TV, Corrin B, Shimosato Y. The new World Health Organization classification of lung tumours. Eur Respir J 2001; 18:1059–68.
36. Germain C, Gnjatic S, Tamzalit F, Knockaert S, Remark R, Goc J, et al. Presence of B cells in tertiary lymphoid structures is associated with a protective immunity in patients with lung cancer. Am J Respir Crit Care Med 2014;189:832–44.
37. Altman DG, Lausen B, Sauerbrei W, Schumacher M. Dangers of using "optimal" cutpoints in the evaluation of prognostic factors. J Natl Cancer Inst 1994;86:829–35.
38. Wemeau M, Kepp O, Tesniere A, Panaretakis T, Flament C, De Botton S, et al. Calreticulin exposure on malignant blasts predicts a cellular anticancer immune response in patients with acute myeloid leukemia. Cell Death Dis 2010;1:e104.
39. Martins I, Kepp O, Galluzzi L, Senovilla L, Schlemmer F, Adjemian S, et al. Surface-exposed calreticulin in the interaction between dying cells and phagocytes. Ann N Y Acad Sci 2010;1209:77–82.
40. Hsu WM, Hsieh FJ, Jeng YM, Kuo ML, Chen CN, Lai DM, et al. Calreticulin expression in neuroblastoma–a novel independent prognostic factor. Ann Oncol 2005;16:314–21.
41. Kageyama S, Isono T, Matsuda S, Ushio Y, Satomura S, Terai A, et al. Urinary calreticulin in the diagnosis of bladder urothelial carcinoma. Int J Urol 2009;16:481–6.
42. Chen CN, Chang CC, Su TE, Hsu WM, Jeng YM, Ho MC, et al. Identification of calreticulin as a prognosis marker and angiogenic regulator in human gastric cancer. Ann Surg Oncol 2009;16:524–33.
43. Eric A, Juranic Z, Milovanovic Z, Markovic I, Inic M, Stanojevic-Bakic N, et al. Effects of humoral immunity and calreticulin overexpression on postoperative course in breast cancer. Pathol Oncol Res 2009; 15:89–90.
44. Liu R, Gong J, Chen J, Li Q, Song C, Zhang J, et al. Calreticulin as a potential diagnostic biomarker for lung cancer. Cancer Immunol Immunother 2012;61:855–64.
45. Senovilla L, Vitale I, Martins I, Tailler M, Pailleret C, Michaud M, et al. An immunosurveillance mechanism controls cancer cell ploidy. Science 2012;337:1678–84.
46. Mlecnik B, Bindea G, Pages F, Galon J. Tumor immunosurveillance in human cancers. Cancer Metastasis Rev 2011;30:5–12.
47. Zitvogel L, Tesniere A, Kroemer G. Cancer despite immunosurveillance: immunoselection and immunosubversion. Nat Rev Immunol 2006;6: 715–27.